JOURNAL OF PROPULSION AND POWER
Vol. 17, No. 3, May–June 2001

Redesigning Gas-Generator Turbines for Improved Unsteady Aerodynamic Performance Using Neural Networks

Nateri K. Madavan* and Man Mohan Rai†
NASA Ames Research Center, Moffett Field, California 94035
and
Frank W. Huber‡
Riverbend Design Services, Palm Beach Gardens, Florida 33418

A recently developed neural network-based aerodynamic design procedure is used in the redesign of a gas-generator turbine stage to improve its unsteady aerodynamic performance. The redesign procedure used incorporates the advantages of both traditional response-surface methodology and neural networks by employing a strategy called parameter-based partitioning of the design space. Starting from the reference design, a sequence of response surfaces based on both neural networks and polynomial fits is constructed to traverse the design space in search of an optimal solution that exhibits improved unsteady performance. The procedure combines the power of neural networks and the economy of low-order polynomials (in terms of number of simulations required and network training requirements). A time-accurate, two-dimensional, Navier–Stokes solver is used to evaluate the various intermediate designs and provide inputs to the optimization procedure. The procedure yields a modified design that improves the aerodynamic performance through small changes to the reference design geometry. These results demonstrate the capabilities of the neural network-based design procedure and also show the advantages of including high-fidelity unsteady simulations that capture the relevant flow physics in the design optimization process.

Nomenclature

c	=	airfoil axial chord
e	=	eccentricity of airfoil leading-edge ellipse
p	=	time-averaged airfoil surface pressure
$\tilde{p}$	=	unsteady pressure amplitude on airfoil surface
t	=	semiminor axis of airfoil leading-edge ellipse
x	=	axial coordinate direction
y	=	transverse coordinate direction
α	=	angular extent of airfoil leading-edge ellipse
β	=	angular extent of airfoil trailing-edge circle

Subscripts

i	=	grid point index
inlt	=	inlet quantity
l, u	=	upper, lower surface of airfoil
min, max	=	minimum, maximum value
rel	=	relative quantity
t	=	total quantity

Introduction

THE aerodynamic design of transonic high-pressure (HP) aircraft engine turbines is complicated by the presence of shocks, wakes, tip leakage, and other secondary flow effects in the flowfield. These shocks, wakes, and vortical flows are ingested by downstream stages, which results in complex interactions with one another and with the flow in these stages. All of these effects are complicated further by the inherent unsteadiness of the flowfield that results from the relative motion of the rotor and stator rows and gives rise to unsteady interactions both within the HP turbine stages and between the HP turbine and the adjacent low-pressure turbine stages. These unsteady interactions may be large enough to affect the time-averaged features of the flow. Cooling and heat transfer are also important considerations in the design process because most HP turbine blades are typically cooled to withstand high operating temperatures. The heat transfer is closely coupled to the unsteady aerodynamics and is often affected greatly by it.

Several experimental investigations of transonic turbines aimed at characterizing shock formation,[1] unsteady stage interactions,[2] heat-transfer effects,[3] and other physical flow phenomena involved have been performed over the years. Various numerical investigations of these flowfields ranging from single blade row computations to time-accurate Navier–Stokes computations in two dimensions,[4–6] and more recently in three dimensions,[7,8] have also added to our understanding of these flows.

Modern HP turbines are usually composed of either one or two stages. Two-stage turbines are longer and heavier but are subsonic and usually more efficient.[8] Single-stage turbines are lighter and compact but operate in the transonic regime and suffer efficiency penalties due to shock losses and high loadings.[8] Even in two-stage designs that are designed to operate in the subsonic regime, there is the potential for unsteady shocks in the flowfield due to high blade loadings. Because of the detrimental effects of these shocks, such as poor aerodynamic performance, unsteady stresses, fatigue, vibration, and reduced blade life, designers have to pay special attention to them. A design optimization method that would help the designers in their efforts to mitigate the effects of these shocks would serve as a very useful tool.

A variety of formal optimization methods have been developed in the past and applied to turbine design. These include inverse-design methods (for example, see Demeulenaere and Van den Braembussche[9]), blade-shape-optimization procedures (for example, see Chattopadhyay et al.[10]), and multidisciplinary-optimization procedures that integrate the heat transfer and aerodynamic effects.[11] The gas turbine industry has also been incorporating design optimization techniques in the turbine design process for some time now.

Presented as Paper 99-2522 at the AIAA/ASME/SAE/ASEE 35th Joint Propulsion Conference and Exhibit, Los Angeles, CA, 20–24 June 1999; received 28 January 2000; revision received 15 June 2000; accepted for publication 11 July 2000.

*Research Scientist, Numerical Aerospace Simulation Systems Division, M/S T27A/1; madavan@nas.nasa.gov.

†Senior Scientist, Information Sciences and Technology Directorate, M/S 269-1; mrai@mail.arc.nasa.gov.

‡President, 4365 Hickory Drive; huberfra@worldnet.att.net.

There are several references in the literature (for example, see Tong and Gregory[12] and Shelton et al.[13]) dealing with the use of a commercially available optimization environment (iSight) in both preliminary design and final design optimization. However, most of this work has its basis in traditional numerical-optimization procedures.

More recently, the authors have developed a different approach to turbomachinery blade design optimization that is based on neural networks.[14,15] This method offers several advantages over traditional optimization procedures. First, neural networks are particularly suitable for multidimensional interpolation of data that lack structure. They can provide a greater level of flexibility than other methods in dealing with design in the context of unsteady flows, partial and complete datasets, combined experimental and numerical data, the need to include various constraints and rules of thumb, and other features that characterize the aerodynamic design process. Second, neural networks provide a natural framework within which a succession of numerical solutions of increasing fidelity incorporating more and more of the relevant flow physics can be represented and utilized subsequently for optimization. Here the term fidelity is used to denote the extent to which the system of equations faithfully represents the physical characteristics of the flow. Third, and perhaps most important, neural networks offer an excellent framework for multidisciplinary-design optimization. Simulation tools from various disciplines can be integrated within this framework. Efficient use can also be made of parallel computing resources. Rapid tradeoff studies across one or many disciplines can also be performed.

Although neural networks have been used in other applications, including aeronautics, for some time now, their application to turbine design optimization is relatively new. Sanz[16] uses a neural network to determine, from a database of input pressure distributions, a pressure distribution that would produce the required flow conditions. An inverse design method is then used to compute the airfoil shape that corresponds to this desired pressure distribution. In other work,[17] although not directly related to neural networks, a turbine aerodynamic design method is developed that is based on an evolutionary optimization technique and uses reinforcement learning to learn adaptively from the design environment.

This paper reports on continuing work by the authors in developing a neural network-based turbomachinery blade design method. It deals with the application of this method[15] to the redesign of a gas-generator turbine with the goal of improving its unsteady aerodynamic performance. The turbine chosen here is a two-stage configuration with an aggressive design characterized by high turning angles and high specific work per stage.[18] Our interest is in the first stage of this configuration. Although the turbine was designed to operate in the high-subsonic regime, an unsteady analysis showed very strong interaction effects including an unsteady moving shock in the axial gap region between the stator and rotor rows. It is hypothesized that the strength of this shock can be reduced by optimizing the airfoil geometries, and the overall unsteady aerodynamic performance of the turbine can thereby be improved. Because the shock can only be discerned by an unsteady aerodynamic analysis, a time-accurate Navier–Stokes solver[19] is coupled to the neural network-based optimizer and provides simulation inputs to it. The results presented here demonstrate that the neural network-based optimization method yields a modified design that is very close to the reference design and achieves the same work output, yet has better unsteady aerodynamic performance because the flow through it is shock free.

The rest of this paper deals with the application of the design optimization method of Rai and Madavan[15] to the redesign of a gas-generator turbine. The design goal is to improve its unsteady aerodynamic performance. Details regarding the redesign procedure and the results obtained are discussed in the following sections.

Reference Design

The turbine that is considered for redesign is a preliminary design developed by Pratt and Whitney for a new generic gas-generator turbine.[18] This turbine is designed to operate in the high subsonic regime and is a two-stage configuration that is characterized by very high turning angles (160 deg in the rotor passage) and high specific work per stage. Further, low-convergence airfoil shapes are used for the rotor blades. All of these features made the design process for this turbine critical. In particular, the 160-deg turning angle was well above most existing designs. Because this design was so far beyond the range of their existing database, the designers were unsure of the effects of unsteady interactions on turbine performance. A post-design unsteady time-accurate analysis of the flow was performed[6] as a final evaluation of the design. This analysis revealed significant unsteady effects and an unsteady shock on the suction surface of the stator that spanned the gap region and impinged on the rotor blades as they passed by the stator airfoils. The position of this unsteady moving shock on the stator suction surface and its strength oscillated periodically in time at blade-passing frequency. The shock is entirely due to the stator–rotor interaction, and any analysis that fails to account for this interaction will fail to indicate the presence of the shock.[6] On the basis of these findings, a design modification that increased the axial gap between the stator and rotor rows (from 30% of mean chord to 75% of mean chord) was recommended. Unsteady analysis of this modified design showed that the flow through the stage was shock free. The uncooled stage efficiency of the modified design was also higher, and the overall performance level was closer to that expected by the designers.

Design Procedure

We use our recently developed neural network-based turbomachinery airfoil design procedure to improve the reference design by successfully mitigating the effects of the unsteady shock. We accomplish our redesign objective by optimizing the shape of the airfoils while maintaining the original axial gap (30% of mean chord). Our purpose is to demonstrate the capabilities of our method for design in an unsteady flow environment and also to show the advantages of capturing the relevant flow physics using high-fidelity unsteady simulations in the design optimization process.

Airfoil Geometry Parameterization

Geometry parameterization and prudent selection of design variables are among the most critical aspects of any shape-optimization procedure. Because this study focuses on airfoil redesign, the ability to represent various airfoil geometries with a common set of geometrical parameters is essential. Variations of the airfoil geometry can be obtained then by smoothly varying these parameters. Geometrical constraints imposed for various reasons, structural, aerodynamic, for example, to eliminate flow separation, etc., should be included in this parametric representation as much as possible. Additionally, the smallest number of parameters should be used to represent the family of airfoils.

The method used for parameterization of the airfoil geometries is described by Rai and Madavan[15] and is reviewed here for completeness. Figure 1 shows the method for a generic airfoil. Some salient features of the method are noted.

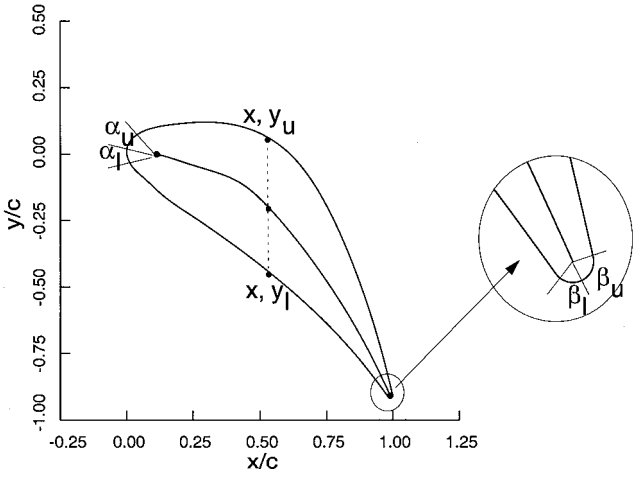

Fig. 1 Schematic of a generic airfoil showing location of control points on the airfoil surface and defining angles used in the parameterization of the airfoil geometry.

First, the leading edge is constructed using two different ellipses, one for the upper surface and one for the lower surface. The eccentricity of the upper ellipse and the semiminor axes of both ellipses are specified as geometric parameters (e_u, t_u, and t_l), respectively. All other related parameters can be determined analytically. The major axes of both ellipses are aligned with the tangent to the camber line at the leading edge. This tangent is initially aligned with the inlet flow but is allowed to rotate as the design proceeds. The angles α_u and α_l determine the extent of the region in which the leading edge is determined by these ellipses. The two ellipses meet in a slope-continuous manner.

Second, the trailing edge can also be constructed in a similar manner with the major axes of the ellipses aligned with the tangent to the camber line at the trailing edge. However, in this study the trailing edge was defined using a single circle. The angles β_u and β_l determine the extent of the region in which the trailing edge is determined by this circle.

Third, the region of the upper surface between the upper leading-edge ellipse and the trailing-edge circle is defined using a tension spline. This tension spline meets the leading-edge ellipse and the trailing-edge circle in a slope-continuous manner. Additional control points for the tension spline that are equispaced in the axial direction are introduced as necessary. These points provide additional control over the shape of the upper surface. The lower surface of the airfoil between the lower leading-edge ellipse and the trailing-edge circle is obtained in a similar manner.

A total of 13 geometric parameters were used to define the stator vane geometries in the current study. These parameters are 1) leading-edge and trailing-edge airfoil metal angles (two parameters), 2) eccentricity of upper leading-edge ellipse (one parameter), 3) angles defining the extent of the leading-edge ellipse (two parameters), 4) angles defining the extent of the trailing-edge circle (two parameters), 5) airfoil thickness values at the leading-edge (two parameters), 6) airfoil y-coordinate values (see Fig. 1) at midchord on the upper and lower surfaces (two parameters), and 7) airfoil y-coordinate values at intermediate points on the upper surface (two parameters).

Because the rotor blade geometries are somewhat more complicated than the stator vane, five additional parameters were required to represent the blades. These parameters were the airfoil y-coordinate values at five additional points on the suction and pressure surface of the blade. Accurate representations of the stator and rotor airfoils in the reference design were obtained using these 13 and 18 parameters, respectively. Acceptable modified airfoil shapes required by the optimization procedure were obtained easily by varying some or all of these parameters.

Unsteady Aerodynamic Analysis

Unsteady aerodynamic analyses of the turbine stage configurations required during the redesign process were obtained using the ROTOR-2 computer code.[19] This code solves the unsteady, two-dimensional, thin-layer Navier–Stokes equations for rotor–stator configurations in a time-accurate manner. Three-dimensional effects of stream-tube contraction are also modeled. The computational method used is a third-order-accurate, iterative-implicit, upwind-biased scheme that solves the time-dependent, Reynolds-averaged Navier–Stokes equations. The ROTOR-2 code has formed the basis of numerous publications (for example, see Refs. 6, 7, 14, 15, and 19). Details regarding the solution methodology, code validation and accuracy studies, and grid refinement issues can be found in these references and the references cited therein.

The flow domain is discretized using a system of patched and overlaid grids; the grids attached to the rotor airfoils can move relative to the grids attached to the stator airfoil to simulate the rotor motion. Figure 2 shows the stator and rotor airfoil cross sections at midspan for the reference turbine design. The reference design has 38 airfoils in the stator row and 52 in the rotor row. To simulate this flow at least 19 stator airfoils and 26 rotor airfoils would have to be modeled as a system.

The computational expense of such a simulation can be reduced considerably by modifying the number of stator airfoils to 39 because this would permit a simulation with 3 stator and 4 rotor airfoils as a system with periodicity conditions to account for the rest of the airfoils. The modification of the stator airfoil count is accomplished by rescaling the stator geometry by a factor of $\frac{38}{39}$ and keeping the pitch-to-chord ratio the same as the actual design. This rescaling is relatively minor and is not expected to alter significantly most of the relevant features of the flow.

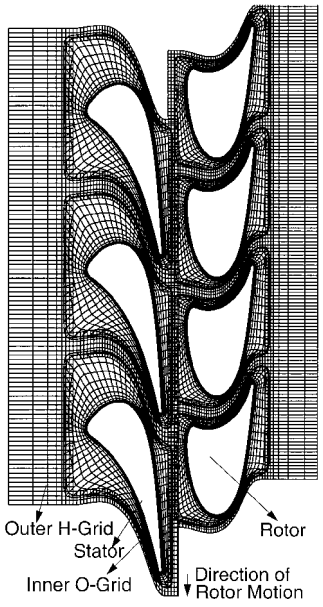

Fig. 2 Turbine geometry (at midspan of reference design) and computational grid used.

Figure 2 also shows the grid system used to discretize the flow domain. Each airfoil has two grids associated with it: an inner O grid that contains the airfoil and an outer H grid that conforms to the external boundaries. For the analyses performed here, each inner O grid has 151 points in the circumferential direction and 41 points in the wall-normal direction. Each outer H grid has 100 points in the axial direction and 71 points in the transverse direction. For the sake of clarity, only some of the grid points are shown in Fig. 2.

The dependent variables are initialized to freestream values, and the equations of motion are then integrated subject to the boundary conditions. The flow parameters that are specified are the pressure ratio across the turbine stage (ratio of exit static pressure to inlet total pressure), the inlet Mach number, the inlet flow angle, and the inlet unit Reynolds number. For the reference design, the pressure ratio across the turbine stage is 0.455, the stator inflow Mach number is 0.0585, the stator inflow angle is 0.0 deg and the inlet unit Reynolds number is 4.9×10^5/in.

Optimization Problem Formulation

The goal of the redesign effort is to improve the unsteady aerodynamic performance of the turbine by optimizing the shape of the stator and rotor airfoils. This is accomplished by formulating an objective function that minimizes the unsteady pressure amplitudes $\tilde{p}_i$ on the stator vane (or rotor blade) subject to the constraint that the tangential force on the rotor airfoil, that is, turbine work output, does not change from the reference design by more than 0.5%. The pressure amplitude $\tilde{p}_i$ is used as a measure of the unsteadiness in the flowfield and is defined as the difference between the maximum and minimum pressures occurring over a complete cycle at each point on the airfoil surface. For the stator vane, a cycle corresponds to the motion of the rotor blade through a distance equal to the rotor pitch. Similarly, for the rotor blade, a cycle corresponds to the motion of the rotor blade through a distance equal to a stator pitch. Thus, the pressure amplitude $\tilde{p}_i$ is defined as

$$\tilde{p}_i = (p_{i,\max} - p_{i,\min})_{\text{cycle}} \tag{1}$$

In the current redesign, the goal is to improve unsteady aerodynamic performance by eliminating the shock. The presence of the unsteady shock in the reference design results in large unsteady

pressure amplitudes. Thus, the pressure amplitudes are directly related to the shock strength. Hence, it is assumed that a reduction in the unsteady amplitudes on the stator vane (and/or rotor blade) will result in a weakened shock. The results obtained demonstrate the validity of this assumption. Note that during the optimization process any modification of either the stator or rotor airfoil geometry could affect the pressure amplitudes on both the stator and the rotor airfoils, due to stator–rotor interaction.

Neural Network-Based Design Procedure

The design procedure used here is that of Rai and Madavan.[15] The procedure uses a sequence of response surfaces based on both neural networks and polynomial fits to traverse the design space in search of the optimal solution. A technique called parameter-based partitioning of the design space is used, where the functional dependence of the variables of interest, for example, pressure, with respect to some of the design parameters is represented using neural networks, and the functional dependence with respect to the remaining parameters is represented using polynomials. The power of neural networks and the economy of low-order polynomials (in terms of number of simulations required and network training requirements) are, thus, effectively combined. The method[15] can be viewed as a variant of response surface methodology[20,21] (RSM), where the response surfaces are constructed using both neural networks and polynomials. Traditional RSM uses only low-order polynomials in constructing the response surfaces.

The method uses polynomial approximations on multidimensional simplexes. An s-dimensional simplex is a spatial configuration of s dimensions determined by $s + 1$ equispaced vertices, on a hypersphere of unit radius. (By this definition, a two-dimensional simplex is an equilateral triangle that is circumscribed by a unit circle.) This approach assumes that the local variation of the design objective function can be accurately represented using low-order polynomials, which is very often the case. The polynomial fit on this simplex, together with the trained neural network, represents a composite response surface. The optimization procedure then uses a sequence of such composite response surfaces to traverse through the design space in search of the optimal solution.

Parameter-based partitioning of the design space is accomplished in the following manner. Because the variation of the unsteady pressure amplitudes along the airfoil surfaces is typically far more complicated than the variation with small changes in geometric parameter values, a neural network is used only to represent unsteady pressure amplitude variation in physical space. The three-layer neural network (with two hidden layers) shown in Fig. 3 is used for this purpose. The first node in the input layer is a bias node (input of 1.0). The second set of nodes is used to specify the physical location. Because we are dealing with two-dimensional geometries only, the physical location is specified by a single parameter, the axial location on the airfoil surface. Figure 3 shows a third set of input nodes that are not activated in this study, but may be used in cases where the functional behavior of the pressure amplitudes with some of the geometric parameters is complex and one wishes to use the neural network to represent this behavior.

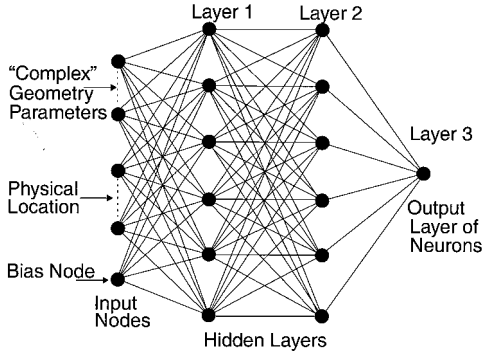

Fig. 3 Schematic of the three-layer feedforward neural network used.

The variation of the unsteady pressure amplitudes with the geometry parameters is approximated using simple polynomials. Because a linear variation is assumed, the points at which the pressure amplitude data are determined are located at the vertices of a simplex of dimension equal to the number of geometry parameters.

The optimization strategy used here to redesign the turbine airfoil geometry starting from the reference design can be summarized as follows.

1) Populate the design space in the vicinity of the reference geometry. The reference design geometry serves as the centroid of the first simplex in the optimization process. A simplex in design space is constructed around this centroid, and unsteady computational fluid dynamics (CFD) analyses at each of the vertices are obtained.

2) Train the neural networks and compute the polynomial coefficients to define the composite response surface. The input nodes of the neural networks will typically contain parameters that correspond to the physical location on the airfoil and those geometric parameters that give rise to complex surface pressure variations. The neural networks are trained, and the polynomial coefficients that define the pressure variation within the simplex are computed. The trained neural networks in combination with the polynomial fit then constitute the composite response surface.

3) Search the region of the design space represented by the composite response surface. A conjugate gradient method was used to perform this constrained search. Geometrical and other constraints can be incorporated within this search procedure easily. In addition, constraints that limit the search procedure to the volume of the simplex are also incorporated in the search.

4) Relocate the simplex. If the local optimum obtained in the preceding step lies on the boundaries of the simplex then this point is chosen as the new centroid and steps 1–4 are repeated until the search culminates inside the simplex. However, the process can be stopped at any time when the design is deemed adequate.

5) Validate the design. As a final step in the process, the unsteady aerodynamic analysis is carried out for the geometry corresponding to the optimal design to determine the adequacy and quality of the design.

Implementation Details

The optimization procedure was initiated from the reference design. The process focused initially on the suction surface of the stator vane. Although 13 geometric parameters were used to represent the stator vane, only 5 of these parameters that were related to defining the suction surface were considered to obtain the modified design. A linear variation of the objective function with respect to the geometric parameters was assumed, resulting in a five-dimensional simplex (with six vertices) at each design optimization step. The process of constructing new simplexes and searching for the local optimum was repeated three times to arrive at the modified design that met the requirement of a shock-free flow. The optimized design was obtained from the modified design by carrying out three additional optimization steps. The first of these steps continued the process of modifying the stator vane geometry, but used six parameters instead of five. In the next two steps, the stator geometry was kept unchanged, and the rotor blade geometry was modified. Unlike the stator geometry modification, the process focused on the leading edge of the rotor blade. Six parameters that were related to defining the rotor leading edge were allowed to vary.

Each of the six three-layer networks (representing the six vertices of the simplex) had two input nodes, one for the bias and one for the axial location, and one output neuron. Both the first and second hidden layers had 11 neurons, for a total of 154 connection weights. Thus, the total number of connection weights for all 6 networks was 924. A sigmoidal activation function was used for all of the neurons. A conjugate gradient-based optimization method was used to train the networks. During the training process, the training error was reduced by about four orders of magnitude from the initial value. The three-layer network architecture was chosen because training times were reduced significantly over that required by two-layer networks.[14]

Results

The neural network-based redesign method was used to optimize the unsteady performance of the reference turbine. This optimization yielded a design (referred to as the modified design) that was close to the reference design, but the unsteady shock was eliminated resulting in better unsteady aerodynamic performance. The modified design was obtained by optimizing the shape of stator vane alone. As a further demonstration, the optimization process was continued by modifying the shape of both the stator vane and rotor blade. The resulting design (referred to as the optimized design) showed further improvements in unsteady aerodynamic performance, but the shape of the stator vane differed noticeably from the reference design. Detailed comparisons of both the modified and optimized designs with the reference design are presented in this section.

Comparison of Stator Vane Geometry for Reference and Modified Designs

Figure 4 compares the stator vane geometry for the reference and modified designs. The geometry of the modified design obtained at the end of the optimization process is very close to that of the reference design. The suction surface has been thinned out in the aft region, and the location of the point where the maximum thickness occurs (the airfoil crown) has moved slightly downstream. Because the geometry modifications are slight, the effect on flow angles and other mean flow parameters is small. However, the impact on the unsteady flow features through the turbine stage is substantial, as the following results will show.

Comparison of Flow Parameters for Reference and Modified Designs

Table 1 compares the flow parameters for the reference and modified designs. The differences between the overall flow parameters in the two cases are very small. This is to be expected because the geometry has been modified very slightly from the reference design.

Static Pressure Variation on Airfoils

Figure 5 shows the time-averaged static pressure variation (normalized by the total pressure at the stator inlet, $p_{t,\text{inlt}}$) on the stator vanes. The static pressure is time averaged over a stator cycle that corresponds to the rotor blades moving by a distance equal to that between adjacent rotor blades, that is, rotor pitch. In the modified design, the pressure minimum near the vane trailing edge is not as low as in the reference design. The vane loading near the midchord region is larger in the modified design.

The variation of time-averaged pressures (normalized by the relative total pressure at the inlet to the rotor row, $p_{t,\text{rel}}$) on the rotor blades is compared for the reference and modified designs in Fig. 6. In this case the time averaging is performed over one rotor cycle,

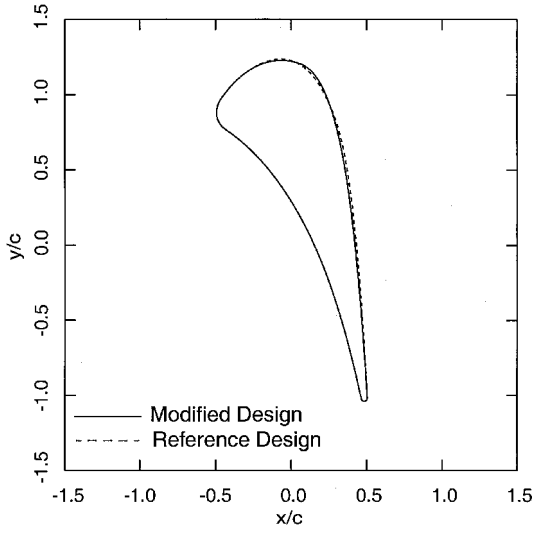

Fig. 4 Comparison of the stator vane geometries for reference and modified designs.

Table 1 Geometry and flow parameters for reference, modified, and optimized designs[a]

Parameter	Reference design	Modified design	Optimized design
Number of stator vanes	38	38	38
Number of rotor blades	52	52	52
Pressure ratio across stage	0.455	0.455	0.455
Unit Reynolds number at stator inlet (per inch), $\times 10^5$	4.9	4.9	4.9
RPM	24,000	24,000	24,000
Ratio of specific heats	1.3699	1.3699	1.3699
Stator inflow Mach number	0.0585	0.0587	0.0587
Stator inflow angle, deg	0.0	0.0	0.0
Stator outflow angle, deg	83.20	83.24	83.18
Rotor-relative inflow angle, deg	79.40	79.37	79.18
Rotor-relative outflow angle, deg	−82.00	−81.98	−82.01

[a]All angles are measured from the axial direction.

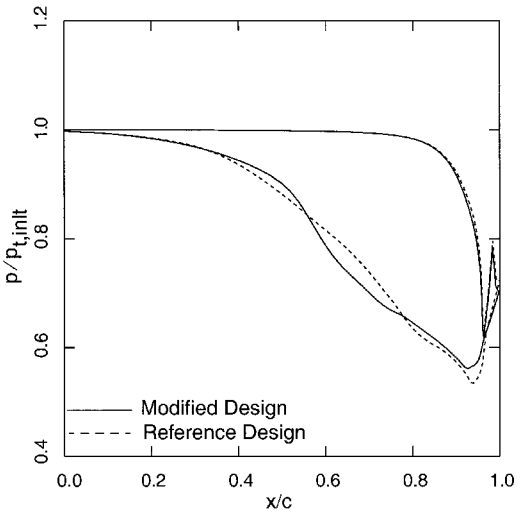

Fig. 5 Comparison of time-averaged pressure distributions on the stator vanes for reference and modified designs.

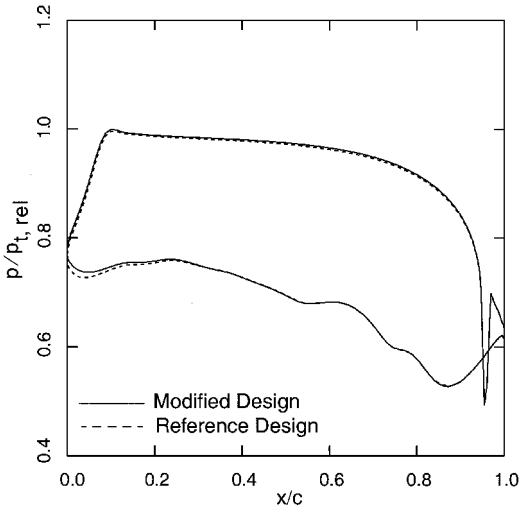

Fig. 6 Comparison of the time-averaged pressure distributions on the rotor blades for reference and modified designs.

which corresponds to the rotor blades moving by a distance equal to that between the stator blades, that is, stator pitch. Because the rotor blade geometry was not modified, the difference in time-averaged pressures between the reference and modified designs is quite small and is limited to the vicinity of the leading edge of the blade.

Instantaneous Contours in the Flow

Figures 7a and 7b compare the instantaneous pressure contours in the flow for the reference and modified designs, respectively. The

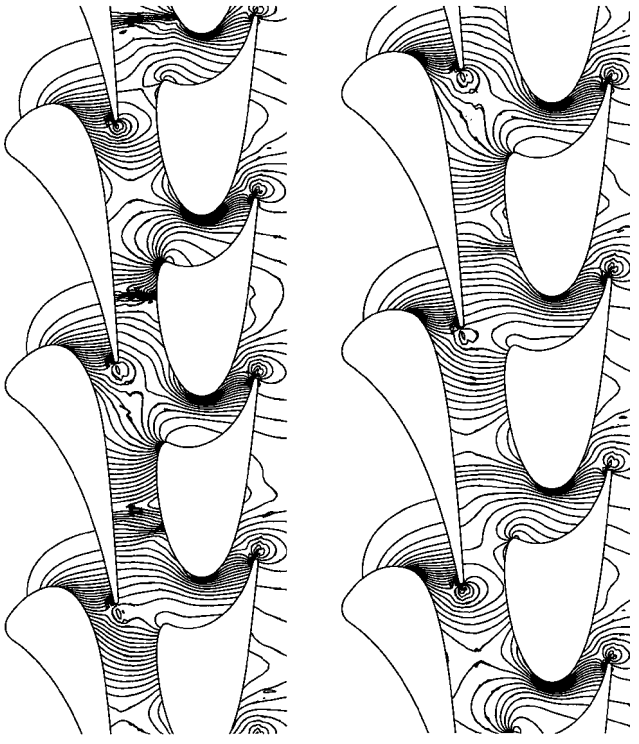

a) b)

Fig. 7 Instantaneous pressure contours in the flow for a) reference design and b) modified design.

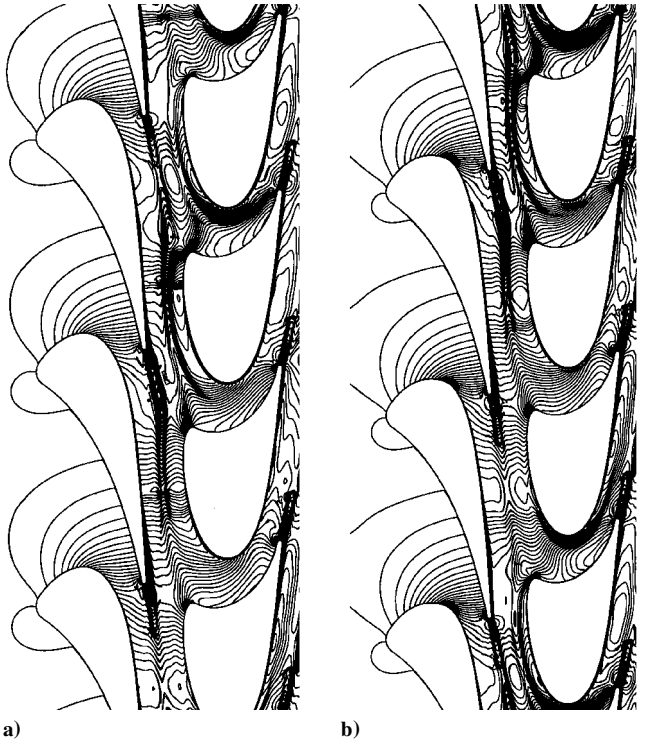

a) b)

Fig. 8 Instantaneous Mach number contours in the flow for a) reference design and b) modified design.

major difference between the reference and modified designs is the unsteady shock in the gap region. This shock can be seen clearly in the reference design, whereas the flow in the modified design is shock free. In the reference design, the shock lies on the vane surface and impinges upon the rotor blades as they pass by the vanes. This unsteady shock, and its motion, is one of the causes of the large temporal pressure variations on the vane and blade surfaces. This shock is entirely due to the interaction between the stator and rotor airfoils. The slight change in the stator vane geometry on the suction side of the modified design effectively eliminates the shock. Figures 7a and 7b represent different instances in the rotor-blade-passing cycle. The time instances correspond to the rotor position when the instantaneous Mach number in the flowfield is maximum and was chosen to represent the worst-case scenario.

Instantaneous Mach number contours are shown in Figs. 8a and 8b for the reference and modified designs, respectively. The maximum instantaneous Mach number is 1.33 in the reference design and 1.13 in the modified design. Whereas pressure contours, in general, highlight only the inviscid aspects of the flow, Mach number contours also highlight the viscous aspects, such as boundary layers and wakes. The shock–wake interaction in the reference design can be clearly seen in Fig. 8a. Despite the unusually high turning angles, the contours show no indication of boundary-layer separation. The instantaneous pressure contours at several representative instances in the rotor-passing cycle showed that the flow was shock free for different relative blade-vane locations. In addition, an animation of the instantaneous flowfield that was created for an optimized design (described in a later section) also showed that the shock had been eliminated over the entire rotor-passing cycle.

Unsteady Pressure Amplitudes on Airfoils

A quantitative measure of the unsteadiness in the flow can be obtained from the unsteady pressure amplitudes on the surfaces of the stator and rotor airfoils. The pressure amplitudes $\tilde{p}$ are defined as the difference between the maximum and minimum pressures occurring over a complete cycle at each point on the airfoil surface [see Eq. (1)]

The pressure amplitudes on the stator vanes for the reference and modified designs are shown in Fig. 9. The abscissa on Fig. 9 is the axial distance x (normalized by the stator axial chord c) along the stator vane measured from the leading edge ($x/c = -1.0$) along the suction surface to the trailing edge ($x/c = 0.0$) and then back to the leading edge along the pressure surface ($x/c = 1.0$). It is evident from Fig. 9 that the large unsteady interaction effects in the reference design have been reduced substantially in the modified design. In particular, the maximum pressure amplitude that is located at the trailing edge of the vane has been reduced by about 30%. As noted earlier,[6] the large pressure amplitudes are caused by the presence of an unsteady moving shock in the gap region. The reduced pressure amplitudes in the modified design indicate that the strength of this shock has been reduced, and its detrimental effects have been mitigated.

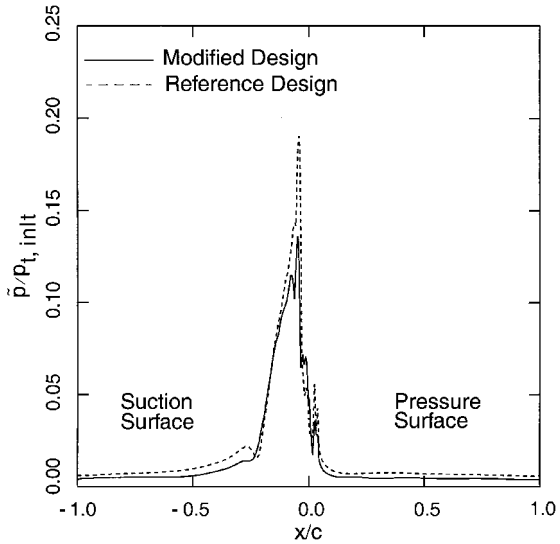

Fig. 9 Comparison of the pressure amplitude distributions on the stator vanes for reference and modified designs.

The pressure amplitudes on the rotor blades for the reference and modified designs are shown in Fig. 10. Unlike in Fig. 9, the abscissa on Fig. 10 is the axial distance x (normalized by the rotor axial chord c) along the rotor blade measured from the trailing

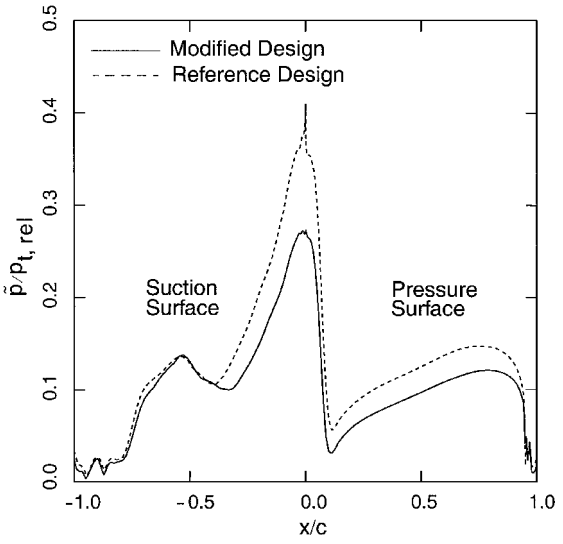

Fig. 10 Comparison of the pressure amplitude distributions on rotor blades for reference and modified designs.

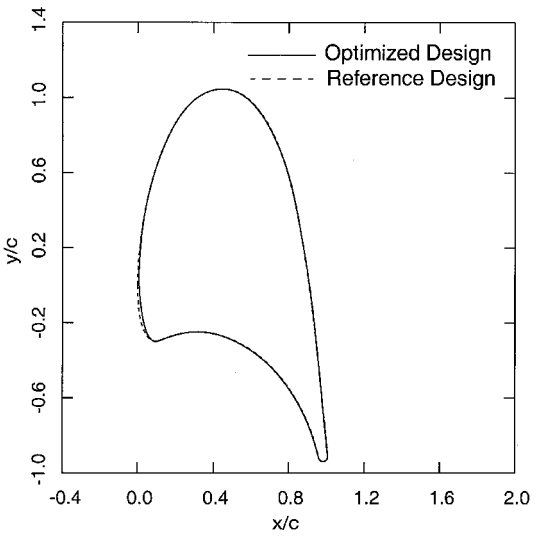

Fig. 12 Comparison of the rotor blade geometries for the modified (unchanged from reference) and optimized designs.

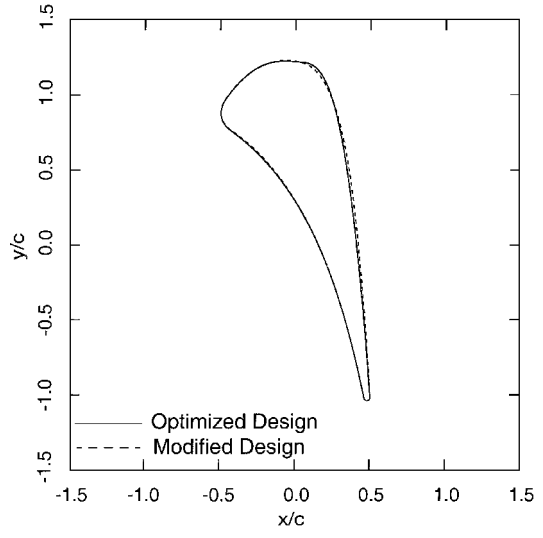

Fig. 11 Comparison of the stator vane geometries for the modified and optimized designs.

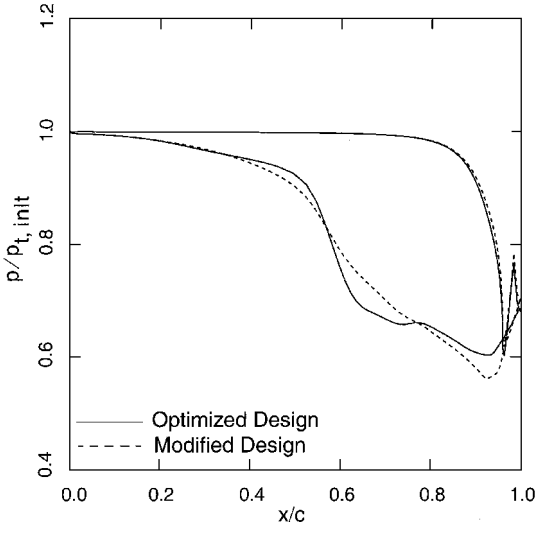

Fig. 13 Comparison of time-averaged pressure distributions on the stator vanes for modified and optimized designs.

edge ($x/c = -1.0$) along the suction surface to the leading edge ($x/c = 0.0$) and then back to the trailing edge along the pressure surface ($x/c = 1.0$). Although the time-averaged pressure on the rotor blade is hardly affected by the stator vane modification, the unsteady pressures on the rotor blades are considerably reduced in the modified design. At the leading edge, the reduction is again about 30%.

Note that the reduction of unsteady effects in the modified design is due primarily to the elimination of the shock. The unsteadiness due to potential and wake–blade interactions between the stator vanes and rotor blades continues to be present because the axial gap between the vanes and blades was not changed in the optimization process.

Further Optimization of the Modified Design

Although the modified design achieved our design objective of a shock-free flow with minimal changes to the stator airfoil geometry, the optimization process was continued beyond this point to explore the possibility of further reduction in unsteady pressure amplitudes by modifying both the stator and rotor geometries. The optimized design that resulted is compared to the modified design next.

Figures 11 and 12 compare the stator vane and rotor blade geometries, respectively, for the optimized and modified designs. The shape of the stator vane in Fig. 11 is noticeably different from the modified design (and the reference design, see Fig. 4). In particular, a flattening of the airfoil crown is noticed on the suction surface. The rotor blade modifications shown in Fig. 12 are quite small.

Figures 13 and 14 compare the time-averaged static pressure variation on the stator vane and rotor blade, respectively, for the modified and optimized designs. The stator suction surface for the optimized design shows an increased loading at about 65% chord and decreased loading toward the trailing edge in comparison to the modified design. This redistribution of the airfoil loading is a continuation of the trend that was observed in obtaining the modified design from the reference design (Fig. 5). The differences in the rotor blade pressure distributions shown in Fig. 14 are quite small and for the most part are confined to the leading- and trailing-edge regions of the suction surface.

Figures 15 and 16 compare the pressure amplitudes on the stator vane and rotor blade, respectively, for the modified and optimized designs. The pressure amplitudes in the optimized design are lower than in the modified design. Recall that the modified design, in turn, had much lower pressure amplitudes than the reference design. The peak pressure amplitude on the stator vane has been reduced from 0.22 in the reference design to 0.14 (36% reduction) in the modified design and to 0.10 (55% reduction) in the optimized design. Similarly, the peak pressure amplitude on the rotor blade has been reduced from 0.40 in the reference design to 0.27 (33% reduction) in the modified design and to 0.20 (50% reduction) in the optimized

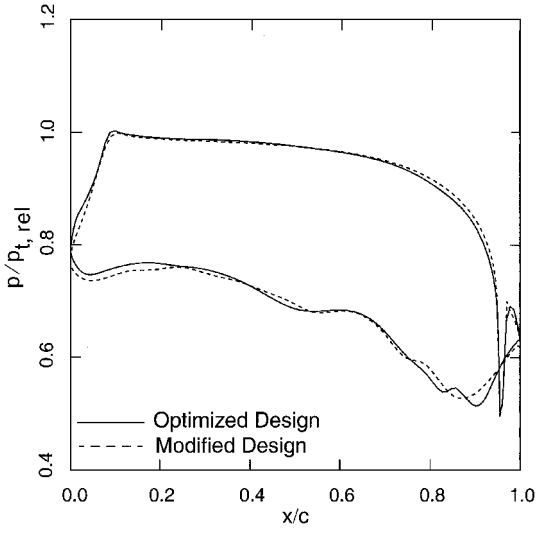

Fig. 14 Comparison of the time-averaged pressure distributions on the rotor blades for modified and optimized designs.

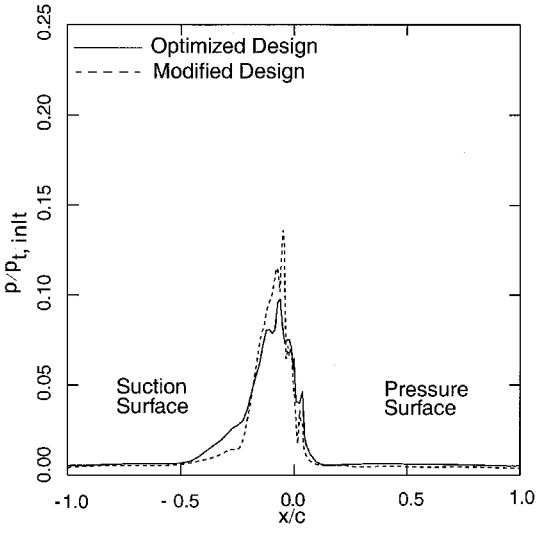

Fig. 15 Comparison of the pressure amplitude distributions on the stator vanes for modified and optimized designs.

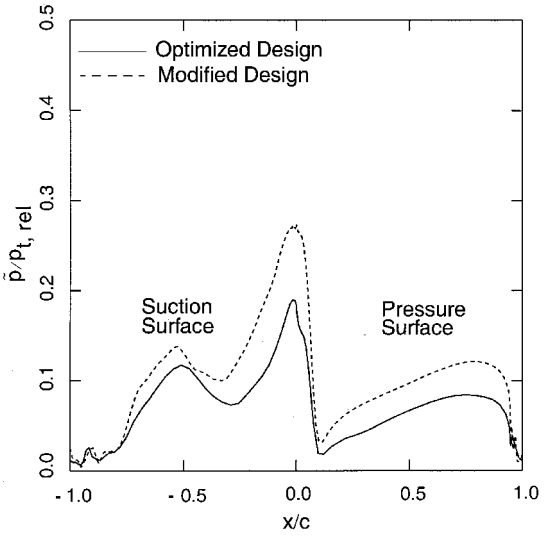

Fig. 16 Comparison of the pressure amplitude distributions on the rotor blades for modified and optimized designs.

design. These reductions in unsteady pressure amplitudes were obtained without changing the tangential force on the rotor blade and the work output of the turbine. For the grid densities used in these computations, the uncooled stage efficiencies for both the modified and optimized designs were also nearly identical to that for the reference design. Efforts are currently underway to compute the uncooled stage efficiencies using more refined grids to further validate these findings.

Convergence and Accuracy of the CFD Simulations

The grid densities used in the CFD simulations for the design optimization studies reported here and in our previous work are typical of those used in the analysis of turbomachinery configurations. It has been our experience in all of these studies that design improvements obtained on these grids are retained when the grids are further refined. This is of considerable importance because it allows design optimization studies to be performed rapidly. The computations on the refined grids also help establish grid convergence. The CFD simulations used in the optimization process were performed on composite grids with about 92,500 grid points. The CFD simulations for the reference and optimized designs were also repeated on a refined grid with about 2.5 times the number of grid points (235,000). Grid refinement yielded nearly identical time-averaged surface pressure distributions for both the reference and optimized designs. However, more sensitive quantities, such as the unsteady pressure amplitudes, did change slightly on grid refinement.

Figure 17 demonstrates that the improvement in flow characteristics obtained through design optimization on the original grid are retained when the flows through the reference and optimized designs are computed on the refined grid. Figure 17 shows the variation of unsteady pressure amplitudes on the rotor blades obtained for the reference and optimized designs on the two different grids. In Fig. 17 only the region of the rotor blade where the pressure amplitudes are substantial is shown. Whereas there are some quantitative differences in the results obtained on the two grids, Fig. 17 shows that the performance improvement obtained through design optimization on the original grid is essentially retained on the refined grid. For example, both the original and refined grid computations show the same reduction (about 0.20) in the peak rotor pressure amplitude in going from the reference design to the optimized design. The grid densities used in the design optimization to obtain the results in the paper are, thus, adequate to resolve the essential features of the flowfield.

Computing Time Requirements

The time required to compute the unsteady CFD simulations represents almost all of the computing time required. The time required to train the neural networks and search the design space is negligible

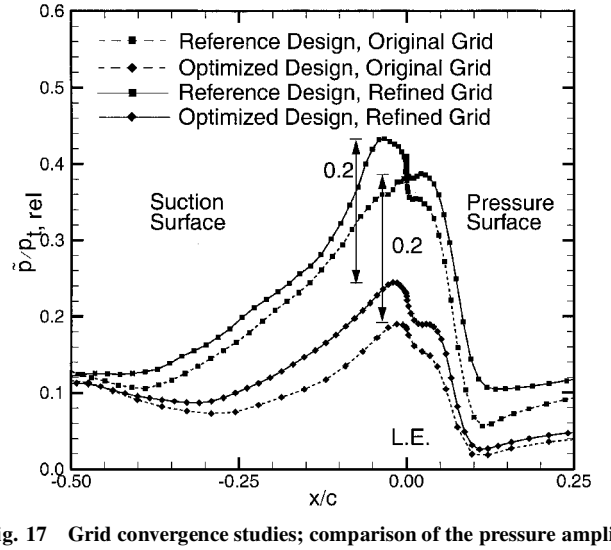

Fig. 17 Grid convergence studies; comparison of the pressure amplitude distributions on the rotor blades obtained on original and refined grids for reference and optimized designs.

in comparison. The modified design was accomplished in three optimization steps, with seven (six vertices plus the centroid) CFD simulations being required at each step. Each CFD simulation required about 5 h of single-processor CPU time on a Cray C-90. The total computing time required to obtain the modified design was, thus, about 100 h. The optimized design required three more optimization steps with eight (seven vertices plus the centroid) CFD simulations being required at each step. Thus, an additional 120 h of computing time were required to obtain the optimized design from the modified design.

Summary

A recently developed method for aerodynamic design that incorporates the advantages of both traditional RSM and neural networks has been applied to the redesign of a gas-generator turbine to improve its unsteady aerodynamic performance. The redesign procedure employs a strategy called parameter-based partitioning of the design space and uses a sequence of response surfaces based on both neural networks and polynomials to traverse the design space in search of the optimal solution. This approach results in response surfaces that have both the power of neural networks and the economy of low-order polynomials (in terms of number of simulations needed and network training requirements). By using high-fidelity, time-accurate Navier–Stokes simulations to steer the optimization process, the relevant physics of the flowfield is included at every stage of the redesign process. The use of such unsteady simulations is mandatory in the current study because the moving shock in the reference design could not be simulated accurately by any other means.

The application of this design method to a reference turbine yielded a new design with a slightly different geometry. Results shown demonstrate that the unsteady shock in the reference design has been eliminated in the modified design. This leads to much lower unsteady pressure amplitudes on the airfoil surfaces and, hence, improved aerodynamic performance. The unsteady pressure amplitudes were reduced even further in the optimized design that was obtained by continuing the optimization process. The shape of the stator vane was altered noticeably from the reference design. These reductions in unsteady pressure amplitudes were obtained without changing the tangential force on the rotor blade and the work output of the turbine. The uncooled stage efficiencies for both the modified and optimized designs were also nearly identical to that for the reference design. These results demonstrate the capabilities of the neural network-based method in design optimization in an unsteady flow environment.

The results presented add to our previous work[14,15] in applying the neural net-based method to design in steady environments and demonstrate the versatility of the method. Although we have used specific design problems as examples to illustrate the strengths of the method, it is clear that the method can be applied to a wide range of turbomachinery and other general design problems.

References

[1]Sieverding, C. H., "Experimental Data on Two Transonic Turbine Blade Sections and Comparison with Various Theoretical Methods," *Transonic Flows in Turbomachinery*, VKI Lecture Series 59, von Kármán Inst., Rhode-St.-Genese, Belgium, 1973.

[2]Ashworth, D. A., LaGraff, J. E., Schultz, D. L., and Grindod, K. J., "Unsteady Aerodynamic and Heat Transfer Processes in a Transonic Turbine Stage," *Journal of Engineering for Gas Turbines and Power*, Vol. 107, No. 4, 1985, pp. 1022–1030.

[3]Guennette, G. R., Epstein, A. H., Giles, M. B., Haimes, R., and Norton, R. J. G., "Fully Scaled Transonic Turbine Rotor Heat Transfer Measurements," *Journal of Turbomachinery*, Vol. 111, No. 1, 1989, pp. 1–7.

[4]Giles, M. B., "Stator/Rotor Interaction in a Transonic Turbine," *Journal of Propulsion and Power*, Vol. 6, No. 5, 1990, pp. 621–627.

[5]Abhari, R. S., Guenette, G. R., Epstein, A. H., and Giles, M. B., "Comparison of Time-Resolved Turbine Rotor Blade Heat Transfer Measurements and Numerical Calculations," *Journal of Turbomachinery*, Vol. 114, No. 4, 1992, pp. 818–827.

[6]Rangwalla, A. A., Madavan, N. K., and Johnson, P. D., "Application of an Unsteady Navier–Stokes Solver to Transonic Turbine Design," *Journal of Propulsion and Power*, Vol. 8, No. 5, 1992, pp. 1079–1086.

[7]Rangwalla, A. A., "Unsteady Navier–Stokes Computations for Advanced Transonic Turbine Design," AIAA Paper 94-2835, June 1994.

[8]Jennions, I. K., and Adamczyk, J. J., "Evaluation of the Interaction Losses in a Transonic Turbine HP Rotor/LP Vane Configuration," *Journal of Turbomachinery*, Vol. 119, No. 1, 1997, pp. 68–76.

[9]Demeulenaere, A., and Van den Braembussche, R., "Three-Dimensional Inverse Method for Turbomachinery Blade Design," *Journal of Turbomachinery*, Vol. 120, No. 2, 1998, pp. 247–255.

[10]Chattopadhyay, A., Pagaldipti, N., and Chang, K. T., "A Design Optimization Procedure for Efficient Turbine Airfoil Design," *Journal of Computers and Mathematics with Applications*, Vol. 26, No. 4, 1993, pp. 21–31.

[11]Talya, S. S., Rajadas, J. N., and Chattopadhyay, A., "Multidisciplinary Optimization of Gas Turbine Blade Design," AIAA Paper 98-4864, Sept. 1998.

[12]Tong, S. S., and Gregory, B. A., "Turbine Preliminary Design Using Artificial Intelligence and Numerical Optimization Techniques," American Society of Mechanical Engineers, ASME Paper 90-GT-148, June 1990.

[13]Shelton, M. L., Gregory, B. A., Lamson, S. H., Moses, H. L., Doughty, R. L., and Kiss, T., "Optimization of a Transonic Turbine Airfoil Using Artificial Intelligence, CFD, and Cascade Testing," American Society of Mechanical Engineers, ASME Paper 93-GT-161, June 1993.

[14]Rai, M. M., and Madavan, N. K., "Application of Artificial Neural Networks to the Design of Turbomachinery Airfoils," AIAA Paper 98-1003, Jan. 1998.

[15]Rai, M. M., and Madavan, N. K., "Aerodynamic Design Using Neural Networks," *AIAA Journal*, Vol. 38, No. 1, 2000, pp. 173–182.

[16]Sanz, J. M., "Development of a Neural Network Design System for Advanced TurboEngines," Fourth U.S. National Congress on Computational Mechanics, Aug. 1997.

[17]Goel, S., and Hajela, P., "Turbine Aerodynamic Design Using Reinforcement Learning Based Optimization," AIAA Paper 98-4774, Sept. 1998.

[18]Johnson, P. D., and Huber, F. W., "GGGT Preliminary Design," United Technologies Pratt and Whitney Memo Pass 57, West Palm Beach, FL, June 1990.

[19]Rai, M. M., and Madavan, N. K., "Multi-Airfoil Navier–Stokes Simulations of Turbine Rotor–Stator Interaction," *Journal of Turbomachinery*, Vol. 112, No. 3, 1990, pp. 167–190.

[20]Montgomery, D. C., *Design and Analysis of Experiments*, Wiley, New York, 1997, Chap. 14.

[21]Myers, R. H., and Montgomery, D. C., *Response Surface Methodology—Process and Product Optimization Using Designed Experiments*, Wiley, New York, 1995.